PERGAMON

International Journal of Heat and Mass Transfer 42 (1999) 4131–4142

International Journal of HEAT and MASS TRANSFER

www.elsevier.com/locate/ijhmt

Theoretical analysis of wafer temperature dynamics in a low pressure chemical vapor deposition reactor

Il-Kyoung Kim, Woo-Seung Kim*

Department of Mechanical Engineering, Hanyang University, 17 Haengdang-dong, Seongdong-ku, Seoul, 133-791, South Korea

Received 24 September 1998; received in revised form 15 February 1999

Abstract

In the LPCVD reactor, temperature variations within the wafer load are the most important factor affecting the film thickness distribution and wafer deformations. In this study the temporal variations of radial and axial temperature nonuniformities of each wafer in the LPCVD reactor are numerically estimated by assuming diffuse reflection. To verify the validity of the present numerical results, the present results obtained from the transient analysis are compared with those of other studies in which a steady-state condition was assumed. The main objective of this work is to determine the temporal variations of the temperature of each wafer in the LPCVD process since the wafers experience severe change in temperature in the early stage of the process. © 1999 Elsevier Science Ltd. All rights reserved.

1. Introduction

In the manufacturing process of wafer, CVD (Chemical Vapor Deposition) process is used mostly to deposit polycrystalline-Si, oxide film, nitride, etc. on the surface of the wafer [1]. The CVD process is classified typically to APCVD (Atmosphere Pressure CVD) process, LPCVD (Low Pressure CVD) process and PECVD (Plasma Enhanced CVD) process. To deposit gases with uniform thickness on lots of wafer surfaces in the environment with temperature of $400 \sim 900^{\circ}C$ and low pressure of 0.2–2 torr, the LPCVD process is generally used [2].

Since in real LPCVD processes it is not easy to predict physical phenomena in the reactor, trial and error methods are used to produce wafers. As the demand for wafer that is larger than 8 inch in diameter increases, it is necessary to understand various problems in the case that the previous multi-wafer LPCVD reactor is used. Thus, for this reason it is very important to appreciate the phenomena in the reactor precisely. There are conditions where wafers experience nonuniform temperature distribution during the process in which wafers are heated and their temperatures increase rapidly.

Sato [3] established the basic radiative properties of silicon at various temperatures and wavelength. Hu [4] proposed a model to describe the transient temperature profile in a row of wafers as they are unloaded from a furnace and cooled to room temperature. He presented a brief analysis that the temperature drop across each wafer (axially) is negligible. Van Schravendijk and De Koning [5] proposed a method for prediction and control of wafer temperatures in a diffusion reactor. They applied the heat balance model to inner elements of reactor like doors, heating coils, process tube and wafers. In their study radial temperature gradients were ignored, and the wafer load was simplified as a cylinder with an appropriately chosen axial thermal

* Corresponding author. Tel.: +82-345-400-5248; fax: +82-345-418-0153.

E-mail address: wskim@email.hanyang.ac.kr (W.S. Kim)

0017-9310/99/$ - see front matter
PII: S0017-9310(99)00069-1

Nomenclature

A_i, A_j	finite surface
c_p	specific heat [J/kg K]
F_{i-j}	view factor
k	conductivity [W/m K]
q_{edg}	heat flux on the edge of wafer
q_i	heat flux
$\dot{q}_z$	boundary conditions of z-direction
R	the radius of wafer
R_i	radiosity
S	the distance of elemental surfaces dA_i and dA_j
$T(r, z)$	temperature
T_{ave}	the average temperature of water
$\overline{T}(r)$	spatially integrated temperature in z-direction
U	the radial temperature nonuniformity

Greek symbols

ε_i	emissivity
θ_i, θ_j	the angle between the surface normal and the line connecting dA_i and dA_j
ρ	density [g/m^3]
ρ_i	reflectivity
σ_T	the standard deviation of radial temperature
$\bar{\sigma}$	Boltzmann constant

conductivity. De Waard and De Koning [6] showed that by assuming diffusely reflecting gray surfaces, the model was simplified enough to allow a description of radiation between all surfaces within the reactor.

Badgwell et al. [7] presented an energy balance model for multi-wafer LPCVD reactors, obtained radial temperature gradients and axial temperature changes of wafer at steady-state by using the orthogonal collocation method numerically. In their work they assumed diffuse reflections between surfaces, since specular and diffuse reflections show similar results in the case the wafer spacing is much smaller than the wafer diameters. Their results agreed well with experimental data.

In this study the temporal variations of radial and axial temperature nonuniformities of each wafer in the LPCVD reactor are numerically estimated by assuming diffuse reflection. To verify the validity of the present numerical results, the present results obtained from the transient analysis are compared with those of Badgwell et al.'s work [7] in which a steady-state condition was assumed. The main objective of this work is to determine the temporal variations of the temperature of each wafer in the LPCVD process since the wafers experience severe change in temperature in the early stage of the process.

2. Modeling of LPCVD reactor

2.1. Analysis of temperature profile

To predict the temperature distribution on each wafer located axisymmetrically in a cylindrical LPVCD reactor, consider the following axisymmetric transient conduction equation [8]:

$$\rho c_p \frac{\partial T}{\partial t} = \frac{1}{r}\frac{\partial}{\partial r}\left(kr\frac{\partial T}{\partial r}\right) + \frac{\partial}{\partial z}\left(k\frac{\partial T}{\partial z}\right) \tag{1}$$

where ρ, c_p, k, t, and T represent density, specific heat, conductivity, time and temperature, respectively.

As shown in Fig. 1 the wafer is a thin disk and since the height of disk, z' is much shorter than the radius of disk R, we can take spatial average on Eq. (1) in z-direction as follows:

$$\frac{1}{z'}\int_{-z'/2}^{z'/2}\rho c_p\frac{\partial T}{\partial t}dz = \frac{1}{z'}\int_{-z'/2}^{z'/2}\left[\frac{1}{r}\frac{\partial}{\partial r}\left(kr\frac{\partial T}{\partial r}\right) + \frac{\partial}{\partial z}\left(k\frac{\partial T}{\partial z}\right)\right]dz \tag{2}$$

Rearranging Eq. (2) makes

$$\rho c_p\frac{\partial \bar{T}}{\partial t} = \frac{1}{r}\frac{\partial}{\partial r}\left(kr\frac{\partial \bar{T}}{\partial r}\right) + \dot{q}_z \tag{3a}$$

where

$$\bar{T} = \frac{1}{z'}\int_{-z'/2}^{z'/2} T\,dz \tag{3b}$$

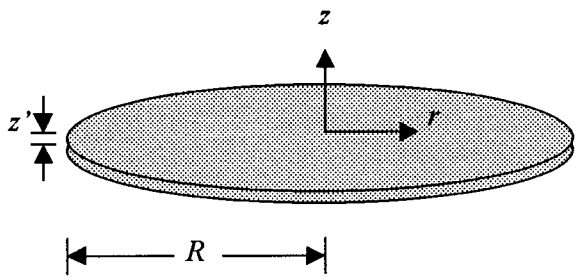

Fig. 1. Coordinate system of wafer.

$$\dot{q}_z = \frac{1}{z'}\left[\left(k\frac{\partial T}{\partial z}\right)_{z'/2} - \left(k\frac{\partial T}{\partial z}\right)_{-z'/2}\right] \tag{3c}$$

Here $\bar{T}$ represents spatially integrated temperature in z-direction, and $\dot{q}_z$ represents boundry conditions of z-direction. The right hand side of Eq. (3c) means heat fluxes to upper and lower surfaces of wafer from the environments. Then, this shows that through the spatial integration Eq. (1) is changed to one-dimensional transient heat conduction equation with source term.

The boundary conditions of Eq. (3a) are symmetric condition at the center of wafer and constant heat flux at the edge of wafer as follows:

$$\frac{\partial \bar{T}}{\partial r} = 0, \quad \text{at } r = 0 \tag{4}$$

$$-k\frac{\partial \bar{T}}{\partial r} = q_{\text{edg}}, \quad \text{at } r = R \tag{5}$$

where q_{edg} represents heat flux on the edge of the wafer.

The governing Eq. (3) is discretized by using the implicit finite difference method [9] with the boundary conditions, Eqs. (4) and (5).

2.2. Simplified zone analysis

Badgwell et al. [7] found experimentally that convective and conductive heat transfer are insignificant at typical LPCVD conditions. This means that heat transfer between surfaces must be dominated by radiation, and heat fluxes at each wafer can be obtained using simplified zone analysis [10].

For analysis of radiative heat exchange in an enclosure (reactor), the entire surface of the enclosure is divided into a finite number of zones and it is also assumed that the following conditions are satisfied at the surface of each zone.

1. The radiative properties are uniform and independent of direction.
2. Either a uniform temperature or a uniform heat flux is prescribed over the surface of each zone.
3. The surfaces are diffuse emitters and diffuse reflectors.
4. The radiosity is uniform over the surface of each zone.
5. The surfaces are opaque.

The simplified zone analysis in an enclosure consists of diffusely reflecting gray-body surfaces and the following equations are satisfied:

$$R_i = \varepsilon_i \bar{\sigma} T_i^4 + \rho_i \sum_{j=1}^{N} R_j F_{i-j} \tag{6}$$

$$q_i = R_i - \sum_{j=1}^{N} R_j F_{i-j} \tag{7}$$

$$q_i = \frac{\varepsilon_i \bar{\sigma} T_i^4 - (1-\rho_i)R_i}{\rho_i}, \quad \rho_i \neq 0 \tag{8}$$

where R, T, q, ε, ρ, $\bar{\sigma}$ and F represent radiosity, temperature, heat flux, emissivity, reflectivity, Boltzmann constant and view factor, respectively. The subscripts i and j denote zone number, and N represents the total number of zones.

By using Eq. (8) radiosity can be represented as an equation with respect to temperature and heat flux as follows:

$$R_i = \frac{\varepsilon_i \bar{\sigma} T_i^4 - \rho_i q_i}{1-\rho_i} \tag{9}$$

Substituting Eq. (6) into Eq. (9), then applying Kirchhoff's law ($\varepsilon = 1-\rho$) and finally rearranging makes the following equation with respect to temperature and heat flux of each zone.

$$\frac{q_i}{\varepsilon_i} - \sum_{j=1}^{N} \frac{1-\varepsilon_j}{\varepsilon_j} q_j F_{i-j} = \bar{\sigma} T_i^4 - \sum_{j=1}^{N} \bar{\sigma} T_j^4 F_{i-j} \tag{10}$$

In Eq. (10) F_{i-j} represents view factor from ith surface to jth surface.

2.3. View factor

Radiative view factor between two surfaces can be formulated as follows:

$$F_{A_i - A_j} = \frac{1}{A_i}\int_{A_i}\int_{A_j} \frac{\cos\theta_i \cos\theta_j}{\pi S^2}\, \mathrm{d}A_j\, \mathrm{d}A_i \tag{11}$$

Many previous studies [11–14] have reported exact solutions of view factors for specific geometries, but it is difficult to find exact solution for general geometry. Specifically, in the case that there are obstacles between two surfaces as in this work, it is difficult to obtain exact solutions of view factors. Hence, for the purpose of obtaining the view factor for general geometry, each surface is divided into finite points, and then view factors can be calculated numerically by the definition given by Eq. (11). For the case with the obstacle between two surfaces, an obstacle detection method can be used to find view factor. Fig. 2 shows the three cases that can occur in detecting an obstacle.

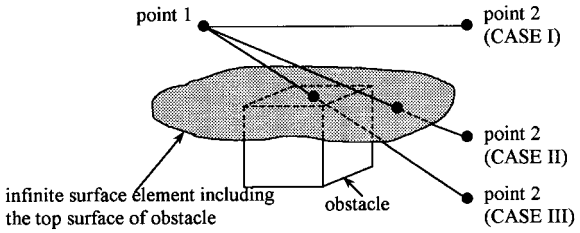

Fig. 2. Three cases in detecting obstacle.

The process of detecting the obstacle between point 1 on surface A_i and point 2 on surface A_j is as follows:

1. Direction vector between two points is calculated.
2. The straight line through point 1 is constructed by using the direction vector.
3. It is assumed that each surface of obstacle is infinite surface element, and it is determined whether the straight line calculated by step 2 crosses this infinite surface element.
4. If the straight line does not cross the infinite surface element (CASE I), the obstacle does not exist between point 1 and point 2. However, if the straight line crosses the infinite surface element (CASE II and III), intersection point is calculated.
5. When the calculated intersection point exists on the real finite surface of obstacle (CASE III), the obstacle exists between point 1 and point 2, and then the integrand of Eq. (11) should be set equal to zero.

3. Results and discussion

3.1. Verification of simulation results

Badgwell et al. [7] used the LPCVD reactor shown in Fig. 3 to numerically analyze the wafer temperature distribution for a hypothetical polysilicon deposition process. Fifty six inch diameter wafers are located axisymmetrically in the reactor. There also exist controllable heaters at the wall of the reactor to constantly maintain the wall with hot temperature. More details on the reactor can be found in reference [7].

The wafer properties used in this simulation are presented in Table 1. It was assumed that the polysilicon film covers the entire surface of wafer and the wall of LPCVD reactor. The emissivity (ε) value of 0.65 was used for all surfaces except doors. The top and bottom doors were assumed to be made of stainless steel with emissivity of 0.37.

In this simulation, an initial temperature of wafers is 30°C and the temperature in the no heater region of reactor's wall is linearly distributed between the temperatures of door and heater. The temperatures of doors are set to 25°C. The temperatures of heater are set to 615°C.

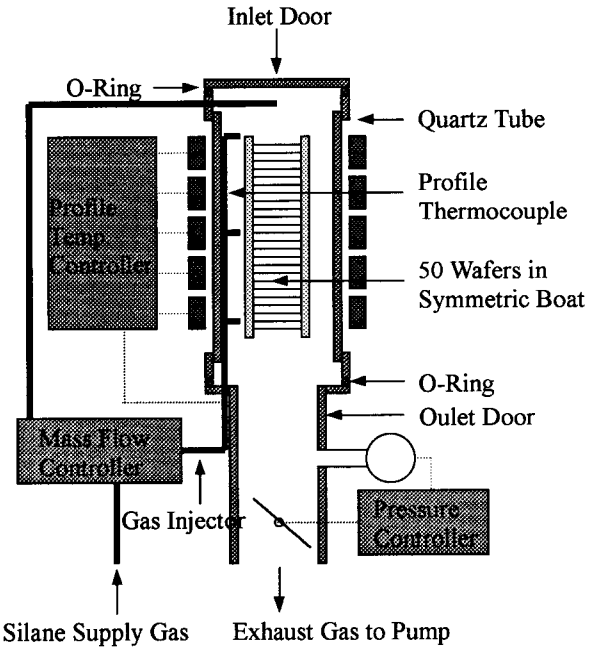

Fig. 3. Vertical multi-wafer LPCVD reactor configuration.

Whereas Badgwell et al. obtained their results from a steady-state energy balance, in the present work steady-state results were obtained through integration of the dynamic system.

Comparisons of average wafer temperature distribution at steady-state between the results of Badgwell et al. and present study are illustrated in Fig. 4. The average temperature is defined as follows:

$$T_{\text{ave}} = \frac{\int_0^R \bar{T}(r) r \, \mathrm{d}r}{\int_0^R r \, \mathrm{d}r} \tag{12}$$

where $\bar{T}(r)$ and R represent the radial temperature and wafer's radius, respectively.

Fig. 4 shows that the average temperature of wafers located at the top and bottom of boat is about 12°C lower than that of wafer near the center of boat. This can be explained by considering the local environment

Table 1
Properties of wafer

Density (ρ)	2.230 g/m^3
Heat capacity (c_p)	932 J/kg K
Thermal conductivity (k)	35.7 W/m K

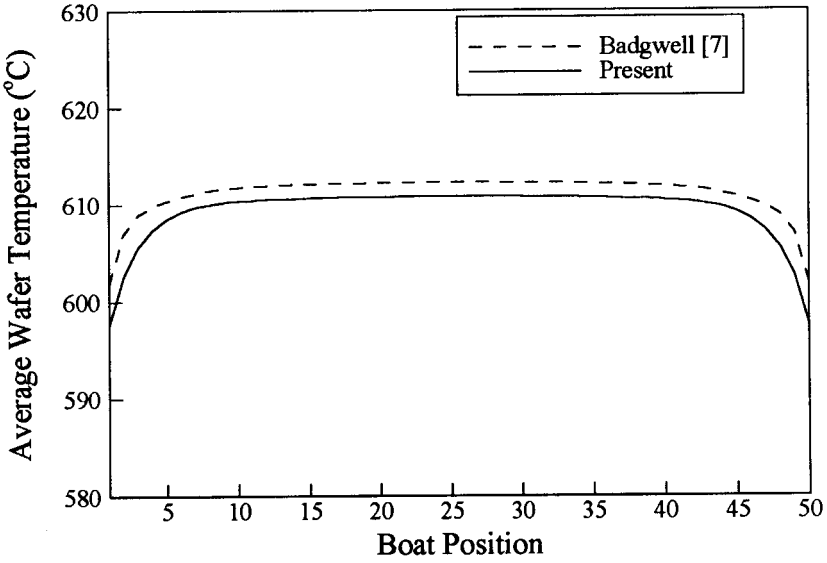

Fig. 4. Average wafer temperature at steady-state.

of each wafer. Comparing with wafers near the center of the boat, the top and bottom wafers receive less energy from the face of the cooler doors of the reactor. Both results of Badgwell et al. and present work show the same trend in the average wafer temperature distribution, but the temperatures predicted by Badgwell et al. are around 2–4°C higher compared to those of present study. It is believed that this small disagreement may be due to the different numerical scheme used by Badgwell et al. to approximate the view factors integrals.

Fig. 5 shows radial temperature nonuniformity at steady-state with respect to wafer position. The radial temperature nonuniformity is the standard deviation of radial temperature divided by average temperature and its definition is as follows:

$$U = \frac{\sigma_T}{T_{\text{ave}}} \tag{13a}$$

where

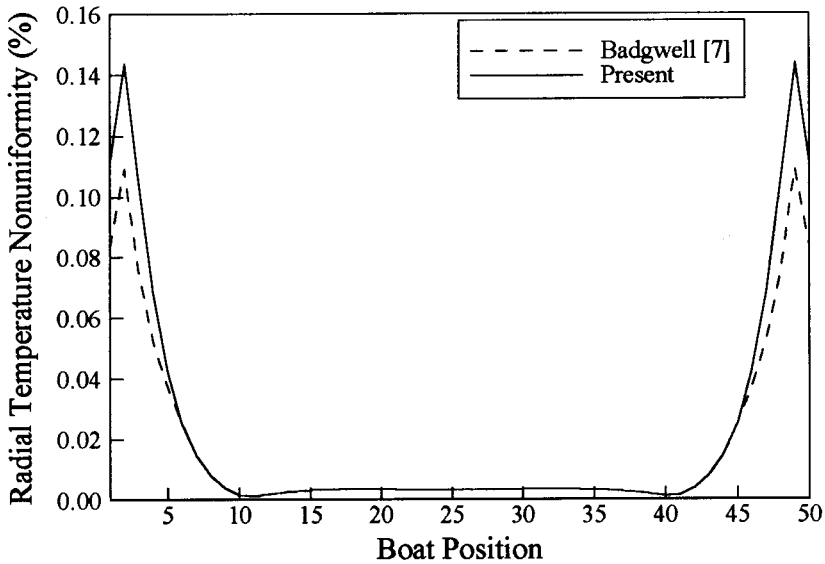

Fig. 5. Radial temperature nonuniformity at steady-state.

$$\sigma_T^2 = \frac{\int_0^R [\bar{T}(r) - T_{ave}]^2 r\,dr}{\int_0^R r\,dr} \tag{13b}$$

In Fig. 5 it is shown that wafers near the ends of the boat have a large nonuniformity. In the meantime, 11th and 40th wafers have the lowest nonuniformity and nonuniformities of the wafers near the center of boat are very small.

Comparison between the present result and that of Badgwell et al. shows that distributions of temperature nonuniformity are similar in both results, but temperature nonuniformities near the both ends of the boat in the present work are about 0.03% larger than those of Badgwell et al. This difference may be attributed to the same fact discussed above.

However, the present prediction through the transient analysis is compared favorably well with the results of Badgwell et al.

The temporal variations of the average temperature of each wafer are presented in Fig. 6. In this simulation it is assumed for simplicity that the wafer stack and reactor are initially at 30°C, and the reactor wall is instantly heated to 615°C. The plot in Fig. 6 indicates that the wafers at the top and bottom of boat experience the highest temperature at the initial stage of the process since one side of these wafers faces the hot wall of the reactor. The temperature of wafers adjacent to the top and bottom wafers increases gradually due to radiative heat transfer between wafers. The wafers near the center of boat experience lower temperature at the beginning of the process since only a few parts of them are exposed to the hot wall of reactor: however, their temperatures increase gradually with time. In the meantime the temperatures of center wafers become higher than those of wafers at both ends of boat, as time elapses more since the end wafers are exposed more to the door maintained at low temperature. The present results indicate that wafers experience considerable change of temperature at the initial stage of process in LPCVD reactor.

Fig. 7 shows the temporal variation of radial temperature nonuniformity in each wafer. In contrast to the results of steady-state, the temperature nonuniformities of the center wafers are considerably large in the early stage of process. This is attributed to the fact that the center wafers at initial temperature of 30°C experience a large temperature nonuniformity since, in the early time, they receive most radiative energy from the hot wall of reactor at the edge of them. However, temperature nonuniformities of the wafers at both ends of boat are smaller than those of center wafers since most parts of the end wafers are exposed to the wall of reactor.

To examine the necessity of transient analysis, temporal variations of temperature drop across the wafer (edge minus center) are presented in Fig. 8 for several wafers located in different positions. Considering the temperature drops in 1st wafer located at the top of the boat, 2nd wafer with the highest radial temperature nonuniformity at steady-state, 11th wafer with the lowest radial temperature nonuniformity at steady-state and 25th wafer located at the center of boat, it is shown that all of the wafers experience a severe temperature drop across the wafer up to about 100 s, then

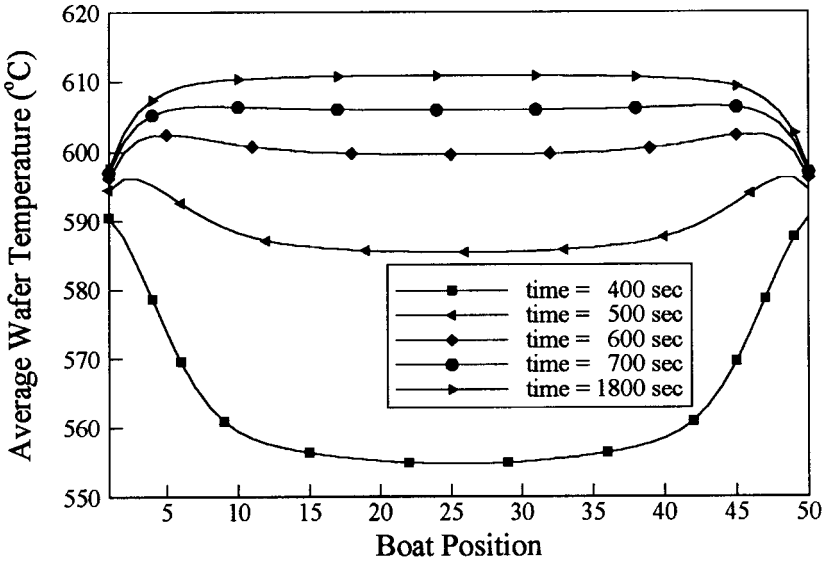

Fig. 6. Temporal variation of average wafer temperature.

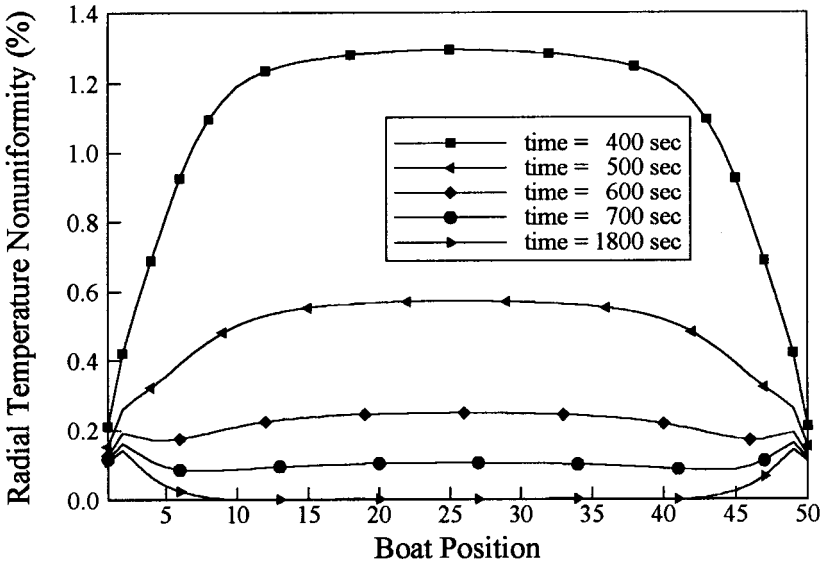

Fig. 7. Temporal variation of radial temperature nonuniformity.

the temperature drop decreases rapidly up to about 600 s and finally after 600 s there is little change in temperature drop.

Fig. 8 also shows that the temperature drops in 11th and 25th wafers are large compared to the other two wafers. This is due to the fact that the edge of these wafers is the main part that is exposed to hot wall of the reactor. It should be noted that the 11th wafer with the lowest radial temperature nonuniformity at steady-state undergoes the highest temperature drop in the early stage of the transient process.

In the next section the present analysis is applied to more realistic process with more than 100 wafers.

3.2. Thermal analysis of the wafers in a more realistic LPCVD reactor

In this section we predict the temporal change of

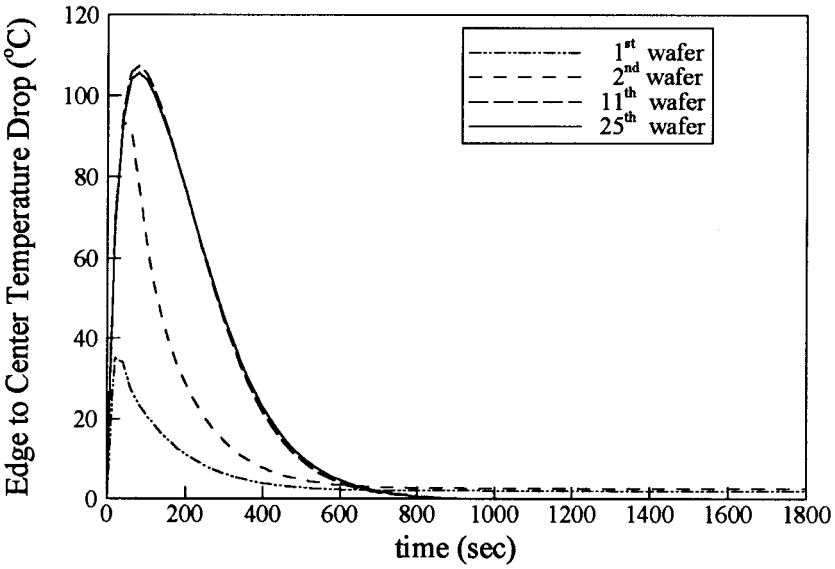

Fig. 8. Temporal variation of temperature drop across the wafers (edge minus center).

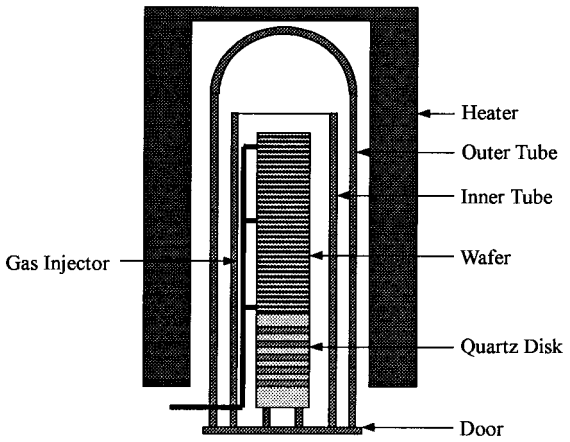

Fig. 9. Schematic diagram of LPCVD reactor considered in this work.

temperature profile of the wafers in a more realistic LPCVD reactor.

The LPCVD reactor considered in this study consists of two quartz tubes, heater, a door and three gas injectors, and boat mounted with 125 wafers and 5 quartz disks located in axis of tube. Fig. 9 shows a schematic diagram of the LPCVD reactor.

Before starting the process the boat moves vertically through the door and it is located in the reactor. Heater temperature is maintained at 440°C before and after the process. The temperature of each heater increases from 440 to 560°C during 15 minutes and then is maintained at 560°C in about 1–2 h. The tube temperature is assumed to be the same as the heater temperature. The door temperature is maintained at about 100°C to prevent the bursting of o-ring. Since door temperature is considerably lower than that of heater, quartz disks are mounted in the lower part of the boat to reduce the effect of door temperature.

Table 2
Dimensions of the LPCVD reactor

Parameters	8 inch wafer	12 inch wafer
Inner tube diameter (mm)	130	195
Profile temperature (°C)	440–560	440–540
Inner tube length (mm)	1157	1157
No. of wafers	125	60
Quartz disk thickness (mm)	2	2
Quartz disk spacing (mm)	6	6
Wafer thickness (mm)	0.725	0.775
Wafer spacing (mm)	5, 6, 7	10
No. of quartz disk	5	5
Door temperature (°C)	100	100

The dimensions and reactor conditions for the 8 inch and 12 inch wafer cases are presented in Table 2. Since the details about 12 inch wafer, dimensions of reactor, and the conditions of process are not published yet, the processing data for 12 inch wafer in Table 2 are generated by scaling-up that for 8 inch wafer.

When the wafer spacing is 7 mm, the temporal variation of the average temperature distribution of all wafers including quartz disks is shown in Fig. 10. The dimensionless boat position of 0 and 1 represents 1st

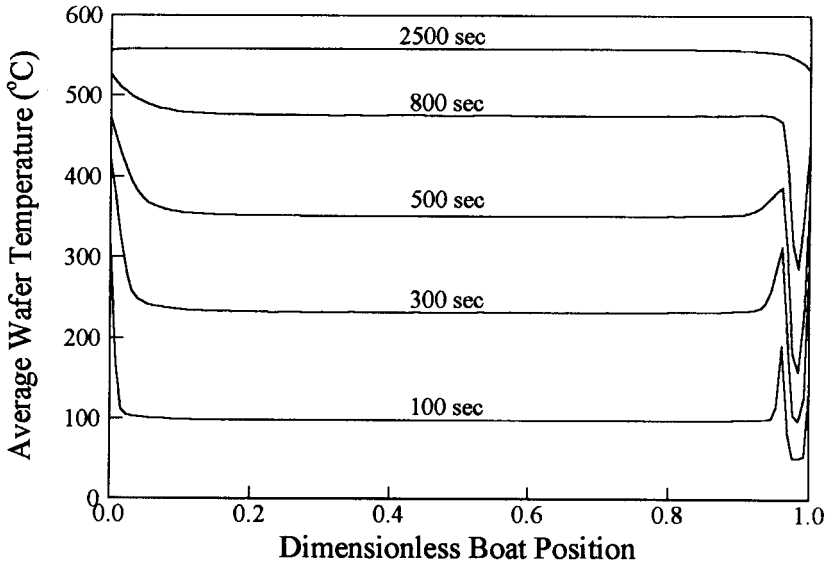

Fig. 10. Average wafer temperature distribution for the case with the wafer spacing of 7 mm.

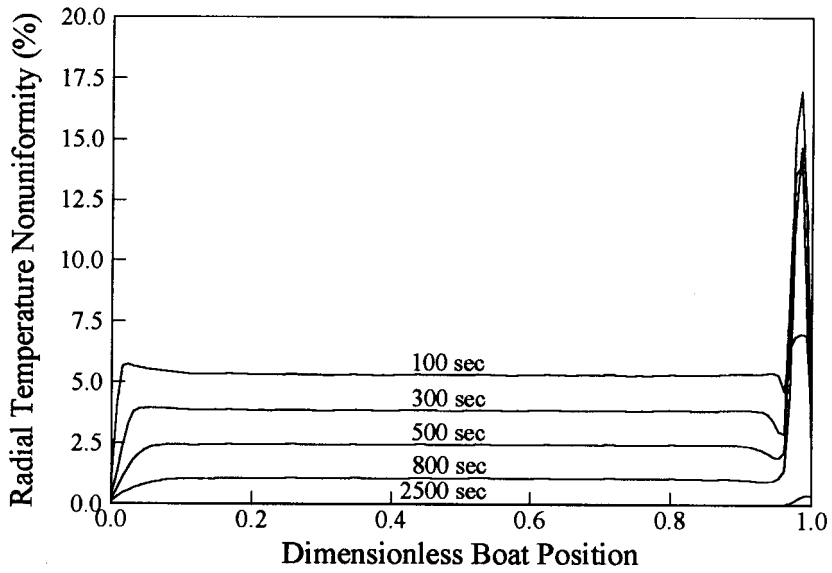

Fig. 11. Radial temperature nonuniformity for the case with the wafer spacing of 7 mm.

wafer and 130th quartz disk location, respectively. As shown in Fig. 10, the last (125th) wafer keeps higher temperature than others in the early time, but its temperature does not increase over 558°C due to the low temperature of the door. The temperatures of wafers which are located below 0.1 and above 0.9 of dimensionless boat position are higher than those of others up to about 1000 s, and the temperatures of the wafers in the center region increase gradually with time.

The average temperature of the wafer at the top of the boat increases rapidly in the early time of the process over the temperature of the wafers in the center region since the wafer at the top of the boat is exposed more to the heaters. However, the increasing rate of the temperature of the 1st wafer decreases with time.

Fig. 11 shows the radial temperature nonuniformity distribution from 100 to 2500 s in the case of the wafer spacing of 7 mm. The average wafer temperature and temperature nonuniformity correlate strongly with average film growth rate and radial film thickness non-

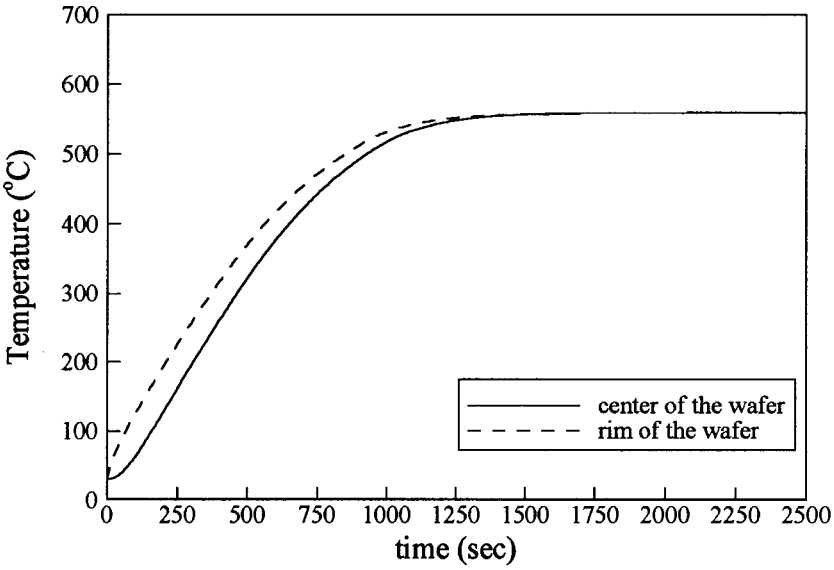

Fig. 12. Transient temperature distribution at the 63rd wafer.

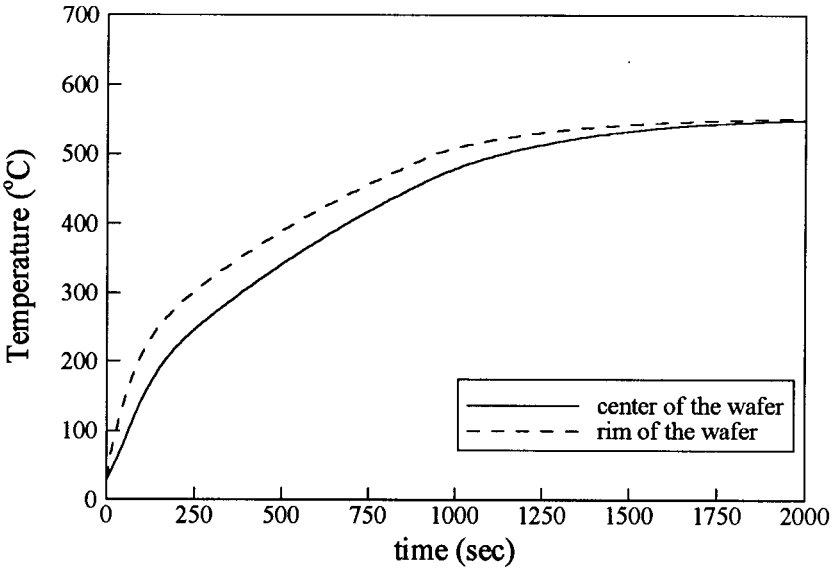

Fig. 13. Transient temperature distribution at the 125th wafer.

uniformity. Temperature deviations of less than about 0.1% are required to get film thickness deviations of no more than 1.0% which are required for 8 inch diameter wafer. However, Fig. 11 indicates that temperature nonuniformity does not decrease to 0.1% up to about 800 s. Proper temperature environment for film thickness uniformity can be obtained after about 1000 s. It is also shown that large temperature nonuniformities occur in quartz disks. This results from the effect of door maintained at a relatively low temperature. Hence, quartz disks improve the temperature uniformities in wafers near the door.

Fig. 12 shows the temporal variations of the temperatures at the center and rim of 63rd wafer that is located in the center of the boat. In the early time the temperature at the rim of the wafer is higher than that at the center of the wafer due to more heat fluxes onto the rim of the wafer. This result indicates that in the starting of the process the center wafers are not stable in the view of the radial temperature nonuniformity.

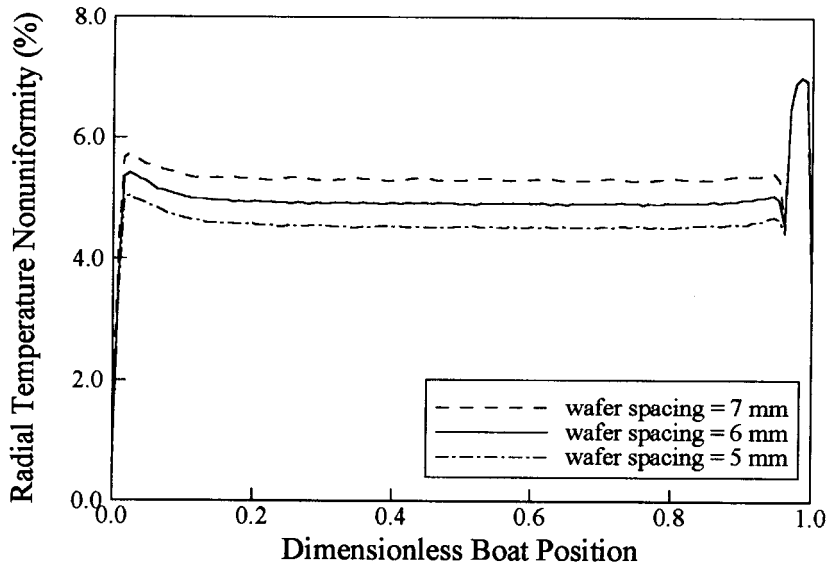

Fig. 14. Radial temperature nonuniformity for different values of wafer spacing at 100 s.

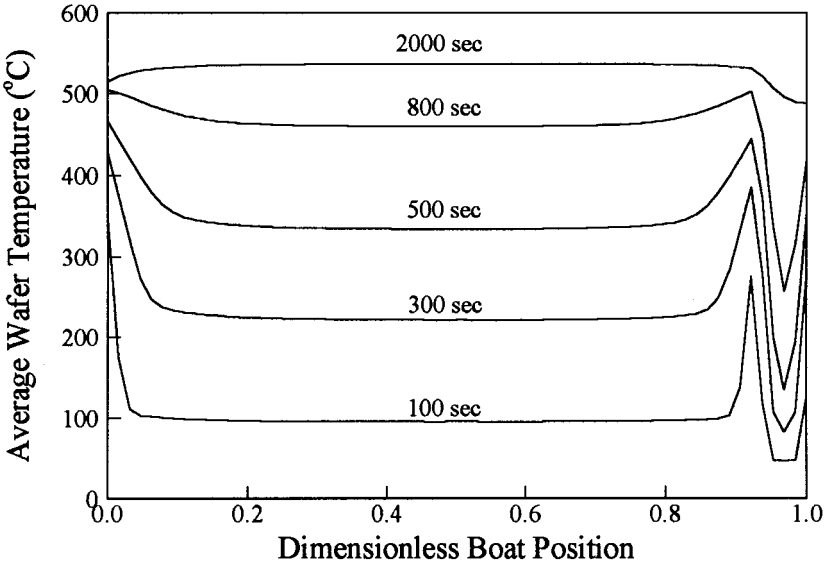

Fig. 15. Average wafer temperature distribution for the 12 inch wafers.

This shows that considering only the temperature nonuniformity at steady-state is inappropriate. It is also shown that there is little difference between them with time.

Fig. 13 represents the temporal variations of the temperatures at the center and rim of 125th wafer. The difference between the temperatures at the center and rim of the 125th wafer at steady-state is larger than that of the 63rd wafer. This results from the fact that the end wafer is exposed more both to the hot wall of tube and to the door with low temperature. It is also shown that the temperature at the rim of the wafer at steady-state is higher than that of the center of it since the center of the wafer is exposed more to the door maintained at low temperature.

Fig. 14 shows the comparison of radial temperature nonuniformities for three wafer spacings of 5, 6 and 7 mm at 100 s. In the case of the wafer spacing of 5 mm the radial temperature nonuniformity is smaller than those of the other cases. This is due to the fact

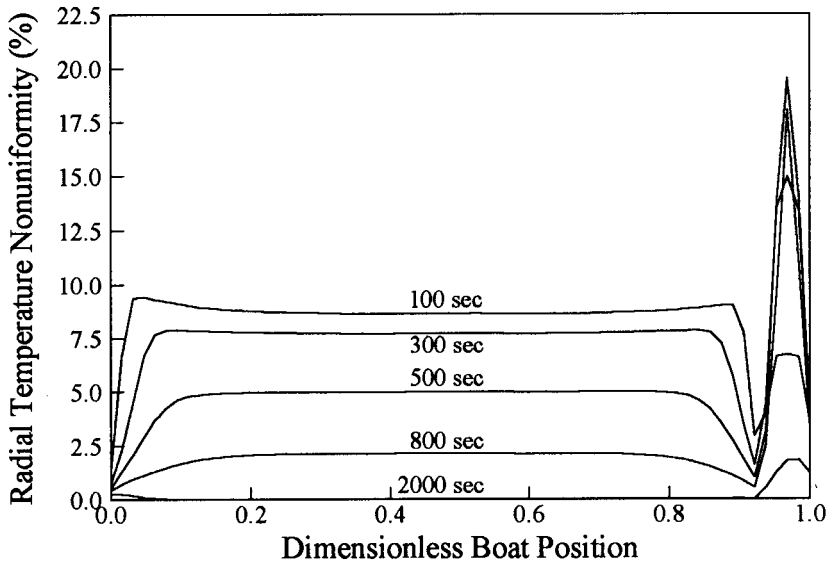

Fig. 16. Radial temperature nonuniformity for the 12 inch wafers.

that in the case with smaller wafer spacing the wafer surface exposure to the door becomes smaller and the radiative heat exchanges between adjacent wafers become more active.

Fig. 15 shows the average wafer temperature distribution from 100 to 2000 s in LPCVD reactor with 60 twelve inch wafers and 5 quartz disks. It is shown that the temperature distribution for 12 inch wafer is similar to the ones for 8 inch wafer in Fig. 10 except for the time required to reach a steady-state.

Fig. 16 shows the radial temperature nonuniformity distribution from 100 to 2000 s. Comparing the present results with the ones for 8 inch wafer in Fig. 11 in the early stage of process, the radial temperature nonuniformity for 12 inch wafer reaches the maximum value of 10%, but 5% for 8 inch wafer. Hence, a simple scaling-up of the dimensions used in 8 inch wafer reactor results in considerably high radial temperature nonuniformity. Therefore, it is necessary to carefully examine the effects of various operating and design parameters on the temperature uniformities of 12 inch wafers.

In most cases of multiwafer LPCVD processes, the occurrence of end effects is observed since the physical characteristics of wafers located at the ends of boat differ from those of most of wafer in boat. For reduction of the end effects, it is necessary to optimize the zone heater temperature, to add more disks as radiation shield, and to use a set of dummy wafers with small spacing.

4. Conclusions

From the transient thermal analysis on the wafers in the LPCVD reactor, the following conclusions are obtained:

1. Transient analysis reveals that the wafers with the most uniform temperature distribution at steady-state have the most non-uniform temperature distribution as the reactor heats up. This is because only the edge of these wafers receives significant radiation from the reactor wall.
2. The radial temperature nonuniformity of each wafer at the early stage of LPCVD process is about forty times higher than that at steady-state.
3. The shorter the wafer spacing becomes, the smaller the radial temperature nonuniformity in the early stage becomes.
4. As to the analysis of temperature field of 12 inch wafer, the scaled-up dimensions of LPCVD reactor may result in magnification of radial temperature nonuniformities of wafers.

Acknowledgement

The authors would like to thank Professor Badgwell for his comments and assistance in preparing this paper.

References

[1] R.S. Rosler, Low pressure CVD processes for poly, nitride, and oxide, Solid State Technology 20 (1977) 63–70.
[2] S.M. Sze, VLSI Technology, McGraw-Hill, New York, 1988.
[3] T. Sato, Spectral emissivity of silicon, Japanese Journal of Applied Physics 6 (1967) 339–347.
[4] S.M. Hu, Temperature distribution and stresses in circular wafers in a row during radiative cooling, Journal of Applied Physics 40 (1969) 4413–4423.
[5] B.J. Van Schravendijk, W.L. De Koning, Modeling and control of the wafer temperatures in a diffusion furnace, Journal of Applied Physics 61 (1987) 1620–1627.
[6] H. De Waard, W.L. De Koning, Optimal control of the wafer temperatures in diffusion/LPCVD reactors, Automatica 28 (1992) 243–253.
[7] T.A. Badgwell, I. Trachtenberg, T.F. Edgar, Modeling the wafer temperature profile in a multiwafer LPCVD furnace, Journal of Electrochemical Society 141 (1994) 161–172.
[8] R. Bird, W. Stewart, E. Lightfoot, Transport Phenomena, John Wiley and Sons, New York, 1960.
[9] K.A. Hoffmann, S.T. Chiang, Computational Fluid Dynamics for Engineers, A Publication of Engineering Education System, 1993.
[10] M.N. Ozisik, Radiative Transfer and Interactions with Conduction and Convection, John Wiley and Sons, New York, 1973.
[11] M.F. Modest, Radiation Heat Transfer, McGraw-Hill, 1993.
[12] R. Siegel, J.R. Howell, Thermal Radiation Heat Transfer, McGraw-Hill, New York, 1982.
[13] J.R. Howell, Radiation Configuration Factor, McGraw-Hill, New York, 1982.
[14] E.M. Sparrow, R.D. Cess, Radiation Heat Transfer, McGraw-Hill, New York, 1976.